IEEE Access
Multidisciplinary | Rapid Review | Open Access Journal

Received July 21, 2019, accepted August 3, 2019, date of publication August 28, 2019, date of current version September 12, 2019.

Digital Object Identifier 10.1109/ACCESS.2019.2938042

Wireless Charging–A Multi Coil System for Different Ground Clearances

DAVID MAIER AND NEJILA PARSPOUR
Institute of Electrical Energy Conversion, University of Stuttgart, 70569 Stuttgart, Germany
Corresponding author: David Maier (david.maier@iew.uni-stuttgart.de)

ABSTRACT Charging electric vehicles wirelessly with inductive energy transfer systems has meanwhile become ready for a widespread practical use. A well known problem is the variation in the magnetic coupling due to the different positions of the vehicle and the ground assembly unit relative to each other. In this work, a method is presented to maintain the input and output current as well as the voltage while changing the ground clearance. For this purpose, a multi-coil system, based on three stacked circular coils, is used. The system has been calculated, simulated and a demonstrator has been built up. Furthermore, a lean system to determine the coupling factor is presented. Measurements, which are showing the satisfactory results, complete the work.

INDEX TERMS Inductive power transmission, mutual coupling, electric variables control, resonance, vehicular and wireless technologies.

I. INTRODUCTION

Nowadays, inductive energy transfer in electric vehicles is beginning to attract more and more attention. Since the standardization is proceeding, it turns out that classes of different vehicle ground clearances will be established [1]–[4] and setups for different vehicle classes as presented in Fig. 1 are possible. From the perspective of the magnetic field, variations in the airgap lead to variations in the coupling factor k, which is calculated with

$$k = \frac{M}{L_1 L_2}, \tag{1}$$

where M is the mutual inductance and L_1 and L_2 are the inductances of the primary and secondary side coil. As a result of the variations in k, undesired side effects appear, such as a change in the output power. To handle the variation in the coupling factor k, different approaches are already known. A first approach refers to the coil system's geometry. The coil geometry can be adjusted with a few single reverse windings to achieve a higher tolerance regarding lateral offset [5] or a complex winding system as presented in [6]–[10] can be used. It is also possible to use electromagnets in the winding system [11] to gain some misalignment tolerance. A second approach solves the different vehicle to ground clearances with the controlling of the primary or the secondary side as it is described in [12], [13] or [14]. In the first case, the controlling is done with hard switching of the power MOSFETs during the energy transfer. However, a continuous control of the system may result in increased switching losses, additional components as well as software effort. Furthermore, mechanical systems, which are actively moving the coil to control the airgap, are used to control the variations in the magnetic coupling [15], [16].

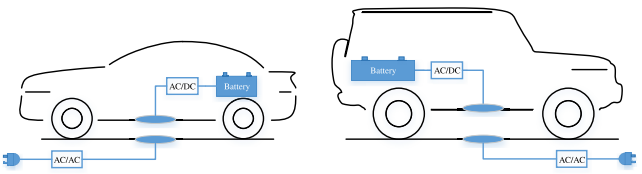

FIGURE 1. Two vehicles with different ground clearances.

In this paper, a novel approach without a continuous controlling or a specific coil geometry is described to handle variations between vehicle and ground assembly. For the following content, the used nomenclature and the system components are presented in Fig. 2.

The paper deals mainly with the coil system in combination with the compensation, which is not described here in detail. Further ohmic losses are not considered in the calculations. The inverter and rectifier as well as the system behavior depending on the compensation are calculated in previous publications [17], [18].

The aim of the work is to maintain the operating point for different ground clearances with a passive approch.

The associate editor coordinating the review of this article and approving it for publication was Abderrezak Rachedi.

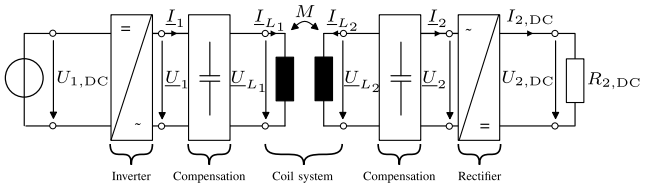

FIGURE 2. Overview of an inductive contactless energy transfer system [17], [18].

For this purpose, the following conditions must be fulfilled for all determined vehicle classes:

- Constant design resonance frequency ω_d
- Constant input voltage $U_{1,\mathrm{DC}}$
- Constant output voltage $U_{2,\mathrm{DC}}$
- Constant transferred power $P_{2,\mathrm{DC}}$

In the following section II, a theoretical consideration with analytical calculations regarding these conditions is presented.

II. THEORETICAL CONSIDERATIONS

Efficient inductive energy transfer is possible with different types of reactive power compensation. For charging electric vehicles, it turned out that a both side serially compensated system is advantageous compared to others [19], [20]. For this reason, the focus in this paper is on serially compensated systems. As described in [17], [18] the input impedance Z_IN and voltage transfer function M_U for the three possible resonant frequencies ω_r0, ω_r1 and ω_r2 are calculated with

$$|\underline{Z}_\mathrm{IN}| = \frac{\omega_\mathrm{r0}^2 k^2 L_1 L_2}{R_2} \quad M_\mathrm{U} = \frac{R_2}{\omega_\mathrm{r0} k \sqrt{L_1 L_2}} \tag{2}$$

for ω_r0 and with

$$|\underline{Z}_\mathrm{IN}| = R_2 \frac{L_1}{L_2} \quad M_\mathrm{U} = \sqrt{\frac{L_2}{L_1}} \tag{3}$$

for $\omega_\mathrm{r1,r2}$. The distinction between the three different resonant frequencies is defined by the characteristic resistance

$$R_{2,\mathrm{c}} \approx k \cdot \omega_\mathrm{d} \cdot L_2 \tag{4}$$

with ω_d representing the selected design frequency. The approximation is well suitable for coupling factors smaller than $k = 0.5$ as described in [18].

As (2) and (4) shows, the equations contain a dependency on the coupling factor k. In Fig. 3, the voltage transfer function is plotted over the load resistance R_2 for three theoretical coupling factors, whereby $k_1 > k_2 > k_3$ applies. Furthermore, an estimated operating point is marked with an *A* inside the figure. The operating point is set next to the value of the characteristic resistance because the system efficiency, considering coil system and reactive power compensation, reaches the maximum at $R_2 = R_{2,\mathrm{c}}$, since the overall reactive power in the system is minimized [21]. The colored areas are representing the typical voltage ranges of a battery. Because the voltage changes during the charging process, the operating point is moving inside the colored area. Considering a

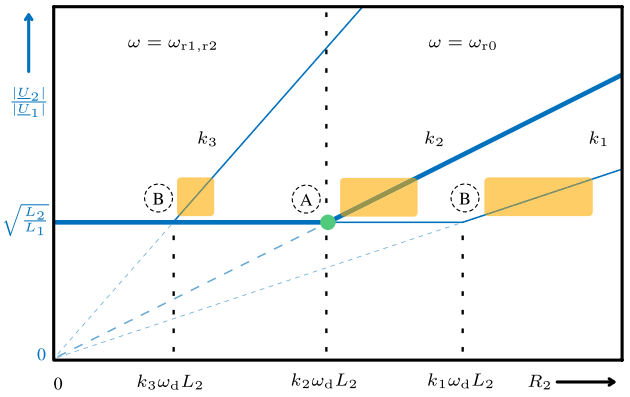

FIGURE 3. Voltage transfer function M_U of a both side serially compensated system for three different coupling factors $k_3 < k_1$; system is designed for operation along the characteristic curve *A*; colored areas next to *A* and *B* show the battery voltage range considering a constant input voltage and thus they represent the operating points for the three coupling factors.

change in the coupling factor, this also leads to a change of the operating point. This behavior is not desired because the efficiency as well as the transferred power changes, wherefore a control system as referenced in section I is needed.

To maintain the operating point with a passive approach, a detailed look on the three equations which describe the operating point is advantageous. The first equation defines the characteristic resistance $R_{2,\mathrm{c}}$ as described in (4). The second equation describes the transferred power

$$P_2 \approx \frac{U_1^2}{k \cdot \omega_\mathrm{d} \cdot L_1} \tag{5}$$

at the operating point $R_2 = R_{2,\mathrm{c}}$ and the last equation describes the voltage transfer function M_U as presented in (2). Considering (2), (4) and (5), it turns out that there is a correlation between the coupling factor k as well as the inductances L_1 and L_2. Since the solution of all three equations must be constant to maintain the operation point, a tuning of both inductors is a good possibility for a passive approach in a both side serially compensated system.

As a result, if the coupling factor k changes, a tuning of both inductors according to the coherence

$$k\uparrow \Rightarrow L_1\downarrow \wedge L_2\downarrow \tag{6}$$

$$k\downarrow \Rightarrow L_1\uparrow \wedge L_2\uparrow \tag{7}$$

is necessary to maintain the operating point. However, a tuning of the inductors results in a change of the resonant frequency

$$\omega_\mathrm{d} = \frac{1}{\sqrt{L_1 \cdot C_1}} = \frac{1}{\sqrt{L_2 \cdot C_2}}, \tag{8}$$

which is not acceptable because of two reasons. First, (4) and (5) vary, if the frequency changes. Secondly, in the course of the standardization process a certain frequency will be specified. As a result, the capacitors must be tuned with the inductors.

If the above mentioned conditions are satisfied, the operating point of the system, which is marked with an *A* in Fig. 3, remains the same.

For other reactive power compensation topologies such as the both side parallel compensated system (1p2p) or a mixed configuration, the coherences are different and they are printed out in Table 1. As it is visible, not all topologies fulfill the requirements. The presented approach is only possible with both side serially or both side parallel compensated systems.

TABLE 1. Parameters of different compensation topologies and impact of a changing coupling factor.

Topology	1s2p	1p2p	1p2s
Parameters[1]			
Output power at $R_{2,c}$	$P_2 \approx \frac{U_1^2}{k \cdot \omega_d \cdot L_1}$	$P_2 \approx \frac{U_1^2 \cdot k}{\omega_d \cdot L_1}$	$P_2 \approx \frac{U_1^2 \cdot k}{\omega_d \cdot L_1}$
Characteristic resistance $R_{2,c}$	$R_{2,c} \approx \frac{\omega_d \cdot L_2}{k}$	$R_{2,c} \approx \frac{\omega_d \cdot L_2}{k}$	$R_{2,c} \approx k \cdot \omega_d \cdot L_2$
Voltage transfer function M_U	$M_U = k\sqrt{\frac{L_2}{L_1}}$	$M_U = \sqrt{\frac{L_2}{L_1}}$	$M_U = \frac{1}{k}\sqrt{\frac{L_2}{L_1}}$
Requirements[2]	$k\uparrow \Rightarrow L_1\downarrow \wedge L_2\uparrow$ $k\downarrow \Rightarrow L_1\uparrow \wedge L_2\downarrow$	$k\uparrow \Rightarrow L_1\uparrow \wedge L_2\uparrow$ $k\downarrow \Rightarrow L_1\downarrow \wedge L_2\downarrow$	$k\uparrow \Rightarrow L_1\uparrow \wedge L_2\downarrow$ $k\downarrow \Rightarrow L_1\downarrow \wedge L_2\uparrow$
Topology fulfills requirements[3]	✗	✓	✗

[1] Analytical calculation without losses [17]
[2] Requirements for a constant P_2 and $R_{2,c}$, assuming U_1 and ω_d are constant in P_2 and $R_{2,c}$.
[3] If the requirements are fulfilled, P_2, $R_{2,c}$ and M_U remain constant.

Another possibility to maintain the operating point with a passive approach, is the tuning of the design frequency ω_d. This approach can only be taken into account if there are no regulations regarding the frequency. The method is especially usable for both side parallel compensated systems with an auto-resonant royer converter, since there are possibilities to connect additional capacitors even during energy transfer [22].

III. SYSTEM DESIGN AND CIRCUIT TOPOLOGY

According to the theoretical considerations in section II, a circuit topology is presented for a both side serially compensated system in this section. Further on, the design of the coil system is printed out and an advice for setting up the coil system is given.

A. CIRCUIT TOPOLOGY

In a practical implementation, the inductor can not be divided into infinitesimal parts to maintain the operating point for every possible coupling factor. As a result, the system is set up for three specific coupling factors, according to the three z-classes mentioned in [1].

Fig. 4 shows a possible circuit design to handle the three different coupling factors to maintain the same operating point as it is printed out with an *A* in Fig. 3.

Fig. 4 shows the primary side on the left and the secondary side on the right. In this setup, only the primary side is controlled, since the secondary side is usually mounted on a car. The car has its specific vehicle to ground clearance and therefore a proper secondary side coil is installed, which matches the primary side. This means that there are three different secondary side coil systems with three different reactive power compensations regarding the ground clearance. Every combination is mounted on the car suitable to the specific z-class. As a result, the primary side has the full control over the charging process and decides autonomously which primary coil fits to the present secondary coil. The method how the primary side detects the present secondary coil is presented in section IV.

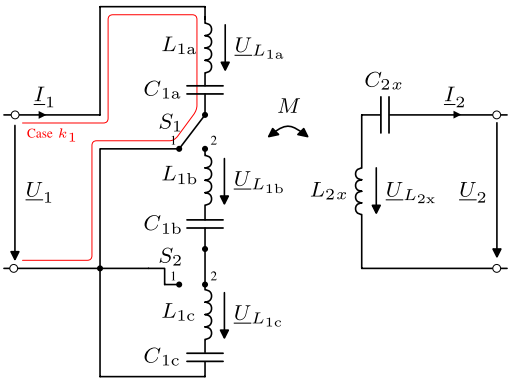

FIGURE 4. Coil system and both side's compensation of the novel system according to Fig. 2; current path for the case with the lowest magnetic coupling k_1 according to Fig. 3 is printed out.

In Fig. 4, two switches S_1 and S_2 are depicted which control the three primary side coils. It is possible to use more than three coils to get a better coupling factor coverage. Independently, the switches are only turned on or off without an active energy transfer. It must be considered that in a serially compensated system a high reactive voltage occurs and the switch has to withstand this voltage. Furthermore, if a classical relay is used, the skin effect in the component must be taken into account. The use of switches to select single coils for positioning tolerant wireless power transfer is already known with a different circuit topology [23], [24].

B. SYSTEM DESIGN

To design the system according to [17], [18], the multi-coil system in Fig. 4 has to be described analytically and must be converted into a single coil system with one coil on each side. The system presented in Fig. 4 contains three primary side coils and one secondary side coil as well as two switches. Hence, there are three possible configurations to transfer energy. In this paper, the analytical calculation of the multi-coil system is only done for the mentioned configurations. For the sake of completeness, a general calculation for multi-coil coupled systems is given in [25].

In the first configuration, the switch S_1 is in position 1 as shown in Fig 4, which means that the voltage U_1 is applied over L_{1a} and C_{1a}. The resulting coil system is analytically

described with

$$\begin{pmatrix} \underline{U}_{\mathrm{L_{1a}}} \\ \underline{U}_{\mathrm{L_{1b}}} \\ \underline{U}_{\mathrm{L_{1c}}} \\ \underline{U}_{\mathrm{L_{2x}}} \end{pmatrix} = \mathrm{j}\omega \begin{pmatrix} L_{1a} & M_{1a1b} & M_{1a1c} & M_{1a2x} \\ \cdots & L_{1b} & M_{1b1c} & M_{1b2x} \\ \cdots & \cdots & L_{1c} & M_{1c2x} \\ \cdots & \cdots & \cdots & L_{2x} \end{pmatrix} \cdot \begin{pmatrix} \underline{I}_{\mathrm{L_{1a}}} \\ \underline{I}_{\mathrm{L_{1b}}} \\ \underline{I}_{\mathrm{L_{1c}}} \\ \underline{I}_{\mathrm{L_{2x}}} \end{pmatrix} \tag{9}$$

The energy transfer happens between L_{1a} and L_{2x}. In this case, the secondary side coil must match the primary side, wherefore the specific coil L_{2a} is used for L_{2x}. The resulting design frequency is calculated with

$$\omega_{\mathrm{d}} = \frac{1}{\sqrt{C_{1a} \cdot L_{1a}}} = \frac{1}{\sqrt{C_{2a} \cdot L_{2a}}} \tag{10}$$

for both sides. Furthermore, the coupling between the two coils is described with

$$k_1 = \frac{M_{1a2a}}{\sqrt{L_{1a} \cdot L_{2a}}}. \tag{11}$$

According to (6) and (7), the above mentioned configuration with the switch S_1 in position 1 is used for the highest of the three coupling factors represented with k_1 in Fig. 3.

In the second configuration for k_2, the switch S_1 is in position 2 and S_2 is in position 1. In this case, the current I_1 flows through L_{1a} and L_{1b}, wherefore (9) simplifies to

$$\begin{pmatrix} \underline{U}_{\mathrm{L_{1a,1b}}} \\ \underline{U}_{\mathrm{L_{1c}}} \\ \underline{U}_{\mathrm{L_{2x}}} \end{pmatrix} = \mathrm{j}\omega \begin{pmatrix} L_{1a} + 2M_{1a1b} + L_{1b} & M_{1a1c} + M_{1b1c} & M_{1a2x} + M_{1b2x} \\ \cdots & L_{1c} & M_{1c2x} \\ \cdots & \cdots & L_{2x} \end{pmatrix} \cdot \begin{pmatrix} \underline{I}_{\mathrm{L_{1a,1b}}} \\ \underline{I}_{\mathrm{L_{1c}}} \\ \underline{I}_{\mathrm{L_{2x}}} \end{pmatrix} \tag{12}$$

In this case, the energy transmitting coil on the primary side consists of L_{1a}, L_{1b} and the mutual inductance M_{1a1b}. It is recommended to have a high coupling between L_{1a} and L_{1b} and thus a high mutual inductance M_{1a1b} because of two reasons. First, with a high coupling, less windings and therefore less copper is used in the system. Secondly, in the case of an error, the resonant frequency of the unused components C_{1c} and L_{1c} differs from (10) and therefore no excitation occurs and no energy transfer is possible within the primary side itself.

Assuming the coupling factors k_2 and k_{1a1b} are known, the value L_{1b}, which is a part of the composed primary side inductor L_1, is calculated with (5) by

$$L_{1b} = \frac{U_1^2}{k_2 \cdot \omega_{\mathrm{d}} \cdot P_1} - L_{1a} - 2 \cdot k_{1a1b} \cdot \sqrt{L_{1a} \cdot L_{1b}}. \tag{13}$$

To achive the same design frequency ω_{d} as in (10), the additional capacitor C_{1b} is defined by

$$C_{1b} = \frac{1}{\omega_{\mathrm{d}}^2 \cdot (2M_{1a1b} + L_{1b})}. \tag{14}$$

If the secondary side coil L_{2b} matches the coupling factor k_2, the setup leads to the same desired operating point A in Fig. 3.

The third configuration for a big airgap, respectively k_3, leads to a coil system with only one coil on each side. In this case, L_{1a}, L_{1b} and L_{1c} are connected by the switches S_1 and S_2 in position 2. This leads to the simplified (15), as shown at the bottom of this page, for the coil system. The calculation of the design frequency ω_{d}, the compensation capacitor C_{1c} and the inductance L_{1c} is carried out in the same way as in the other cases.

C. COIL DESIGN

For the prototype, a circular coil system is used. According to section III-B, a high coupling factor between the primary side coils is desirable. Since there are several possibilities to arrange the three primary side coils, a finite element analysis was done with several coil arrangements. It turned out that a three layer primary side coil with a commonly distributed winding is a reasonable choice. The favored arrangement is shown in Fig. 5 along with the three different coils A, B and C which represent L_{1a}, L_{1b} and L_{1c} of Fig. 4. The coils are distributed as shown in the left hand side of the figure to achieve the highest coupling between the single coils. The presented coil arrangement is only one possibility, there are countless possibilities to design the coil system beside circular coil systems. The arrangement of the coils is not important for the function of the novel system. Nevertheless, a high coupling leads to a better efficiency, since the resistance of the coil system is smaller and thus the quality factor is higher.

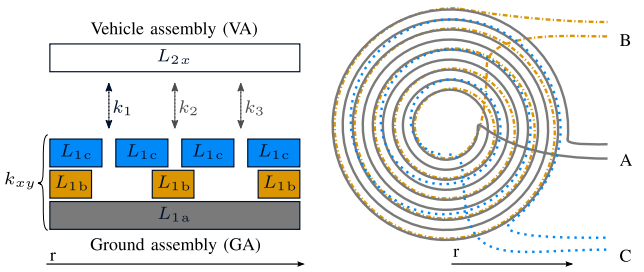

FIGURE 5. Coil arrangement with a coupling factor $k \approx 0.94$ between the coils *A*, *B* and *C*.

IV. METHODS TO MEASURE THE COUPLING FACTOR

Along with different vehicle ground clearances, a method for measuring the coupling factor must be found to properly switch the primary side coil regarding the position of the car.

$$\begin{pmatrix} \underline{U}_{\mathrm{L_{1a,1b,1c}}} \\ \underline{U}_{\mathrm{L_{2x}}} \end{pmatrix} = \mathrm{j}\omega \begin{pmatrix} L_{1a} + L_{1b} + L_{1c} + 2M_{1a1b} + 2M_{1a1c} + 2M_{1b1c}M_{1a1x} + M_{1b2x} + M_{1c2x} \\ \cdots \qquad\qquad\qquad\qquad\qquad\qquad\qquad\qquad\qquad\qquad\qquad\qquad\qquad\qquad L_{2x} \end{pmatrix} \cdot \begin{pmatrix} \underline{I}_{\mathrm{L_{1a,1b,1c}}} \\ \underline{I}_{\mathrm{L_{2x}}} \end{pmatrix} \tag{15}$$

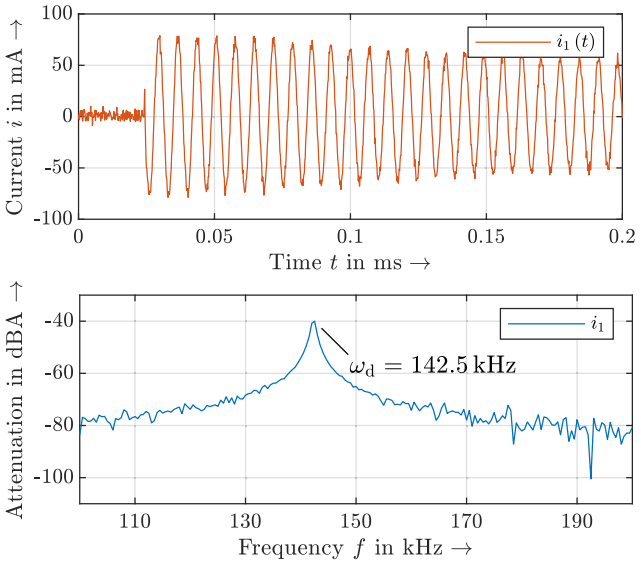

FIGURE 6. Measurement with opened secondary side $R_2 = \infty$; measured current I_1 of the step response in the top and corresponding FFT over 2 ms respectively 500 Hz resolution in the bottom.

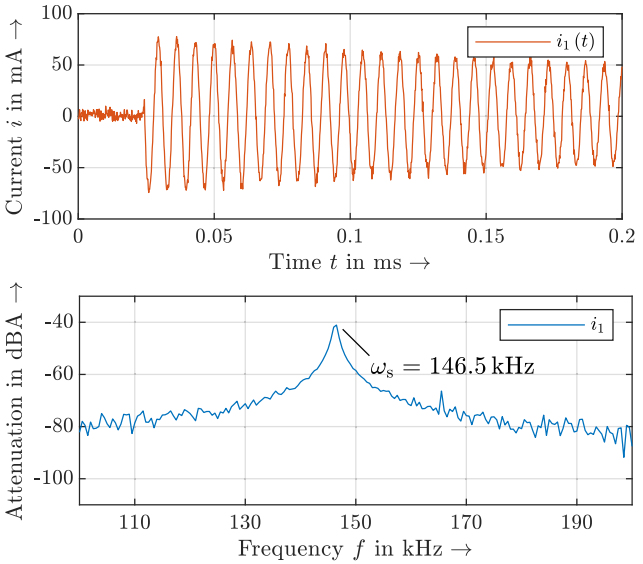

FIGURE 7. Measurement with a short circuited secondary winding L_2; measured current I_1 of the step response in the top and corresponding FFT over 2 ms respectively 500 Hz resolution in the bottom.

For that reason, the magnetic parameters of the system have to be estimated. For WPT systems, there are already different approaches [26]–[29] known. Basically, a distinction is made between measuring the coupling factor during energy transfer and without energy transfer. In the specific case described in this paper, a measurement without energy transfer is needed. Therefore, several options are possible. Since a common LCR meter is not suitable for commercial use, a novel method based on analyzing the step response is used for this application.

Analyzing the step response to obtain the coupling factor k requires at least two measurements. In Fig. 6 the step response and the corresponding fast Fourier transformation (FFT) of the open circuit are presented. For the FFT, a time frame of 2 ms with a rectangular window function was used. The measurement itself has been done with a Yokogawa DLM4000 oscilloscope. Referring to Fig. 2, the capacitors of the rectifier must be pre-charged or the rectifier must be disconnected to achieve an open circuit behavior with $R_2 = \infty$. To measure the decay behavior properly, a voltage jump of 5 V and 0.5 Hz is applied. Since current is easier to measure in a both side serially compensated system, the current measurement $i_1(t)$ was used for the FFT. Albeit, measuring the voltage U_{L_1} would lead to the same solution. The minimum attenuation in Fig. IV shows the design frequency

$$\omega_d = \frac{1}{\sqrt{C_1 \cdot L_1}} \tag{16}$$

of the CET system.

To calculate the coupling factor, a second measurement is needed. There are at least two possibilities. On the one hand, the step response with a short circuit over L_2 can be analyzed and on the other hand, the step response with a short circuit over both L_2 and C_2 can be evaluated. Each of the methods has respective advantages. The first method is presented in Fig. 7. As it is visible in the time domain, the frequency could be determined without implementing a FFT with a simple zero crossing detection. However, a short circuit is not easy to implement in a practical system. According to [18], the coupling factor is calculated with

$$k = \sqrt{1 - \frac{L_{1s}}{L_1}} \tag{17}$$

respectively with (16) to

$$k = \sqrt{1 - \frac{\omega_d^2}{\omega_s^2}} \tag{18}$$

where ω_s is the frequency with minimum attenuation of Fig. 7.

The second method provides two frequencies and therefore a FFT must be done. The time and frequency domain are presented in Fig. 8. According to [17] the resonant frequencies ω_{r1} and ω_{r2}, further referred to by $\omega_{r1,r2}$, are calculated with

$$\omega_{r1,r2} = \frac{\omega_d}{\sqrt{1 - \frac{R_2^2}{2 \cdot \omega_d^2 \cdot L_2} \pm \sqrt{\left(1 - \frac{R_2^2}{2 \cdot \omega_d^2 \cdot L_2}\right)^2 - \left(1 - k^2\right)}}} \tag{19}$$

for a both side serially compensated system. In case of a short circuit $R_2 = 0$ across L_2 and C_2, (19) simplifies to

$$\omega_{r1,r2} = \frac{\omega_d}{\sqrt{1 \pm k}}. \tag{20}$$

As a consequence, the coupling factor k is calculated with

$$k = \left|1 - \frac{\omega_d^2}{\omega_{r1}^2}\right| = \left|1 - \frac{\omega_d^2}{\omega_{r2}^2}\right|. \tag{21}$$

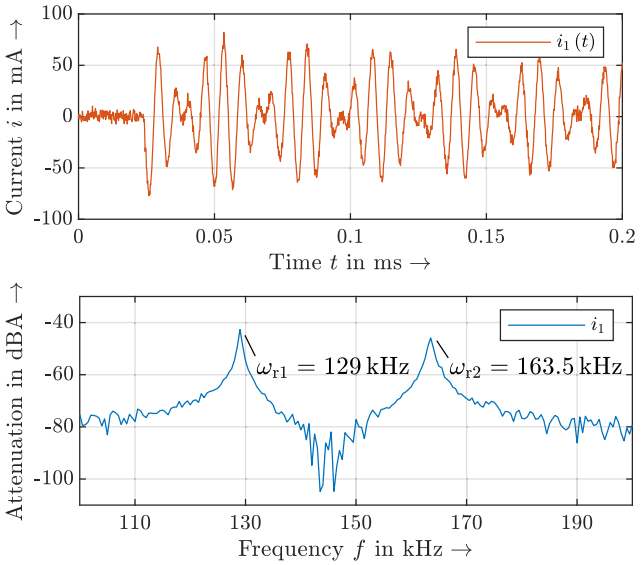

FIGURE 8. Measurement with a short circuit over L_2 and C_2; measured current I_1 of the step response in the top and corresponding FFT over 2 ms respectively 500 Hz resolution in the bottom.

The frequencies $\omega_{r1,r2}$ are gained by selecting the two values with minimal attenuation of the FFT in Fig. 8. The values can both be used to calculate k with (21). It is advisable to use the average value of both solutions due to measuring errors. The results of the three presented measurements are pooled in Table 2. It is visible that every method leads to nearly the same coupling factor. Furthermore, the mean value of the coupling factor is identical to the measurement with a common LCR meter by using (17).

TABLE 2. Measured frequencies to determine k for the three different coil systems.

Configuration	Setup 1	Setup 2	Setup 3
Measured values			
Airgap	4 cm	6 cm	10 cm
Frequency ω_d	142.5 kHz	142.5 kHz	142.5 kHz
Frequency ω_s	152.5 kHz	146.5 kHz	143.5 kHz
Frequency ω_{r1}	122 kHz	129 kHz	134.5 kHz
Frequency ω_{r2}	177.5 kHz	163.5 kHz	152.0 kHz
Calculated values with FFT			
Coupling k^1	0.3562	0.2321	0.1179
Coupling k^2	0.3643	0.2203	0.1225
Coupling k^2	0.3555	0.2404	0.1211

[1] Calculated with (18).
[2] Calculated with (21).

V. SETUP AND MEASUREMENTS

In this section, the setup and measurements are presented. For the demonstration of the described system, a prototype is built up. To demonstrate the function, a power transfer of only 50 W at 24 V was chosen because it is cost efficient and the system should operate with safety extra-low voltage for demonstration purposes. In a next step, the system can be built up with 3.6 kW or more. The parameters of the prototype are given in Table 3. The values are divided into the calculated

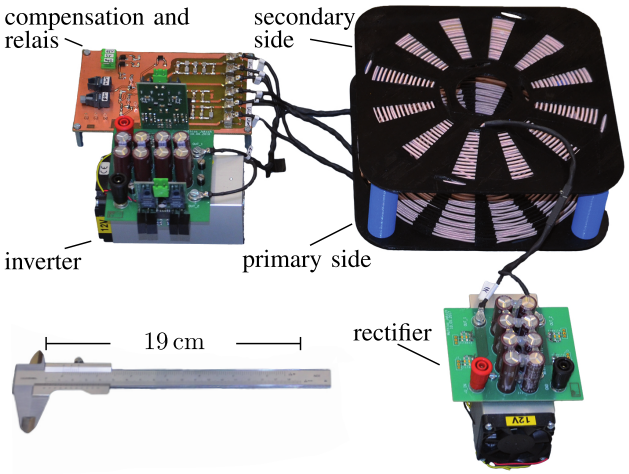

FIGURE 9. Hardware setup of the demonstrator; primary side power electronics and reactive power compensation capacitors on the left side, rectifier at the bottom and coil setup at the top right corner.

TABLE 3. Parameters of the prototype system.

Parameter	Value Calculated/Measured	Parameter	Value Calculated/Measured
P	50 W[1]	f_d	142.5 kHz
U_1	25.7 V[1]	$U_{1,DC}$	28.7 V[1]
U_2	25.7 V[1]	$U_{2,DC}$	28.7 V[1]
k_1	0.36/0.36	z_1	10 cm
L_{1a}	41.39/41.4 µH	C_{1a}	30.13/31.0 nF
L_1	41.39/41.4 µH	C_1	30.13/31.0 nF
L_2	41.39/40.2 µH	C_2	30.13/30.5 nF
k_2	0.20/0.22	z_2	6 cm
L_{1b}	5.29 µH[3]	C_{1b}	37.66/38.1 nF
L_1[2]	74.52/72.8 µH	C_1	16.74 nF[3]
L_2	74.52/72.0 µH	C_2	16.74/37.6 nF
k_3	0.10/0.12	z_3	4 cm
L_{1c}	13.71 µH[3]	C_{1c}	16.74/17.1 nF
L_1[2]	149.03/146.7 µH	C_1	8.37 nF[3]
L_2	149.03/145.8 µH	C_2	8.37/8.66 nF

[1] Measured values are shown in the measurement figures.
[2] Coupling between L_{1a}, L_{1b} and L_{1c} for calculation is k=0.94.
[3] Value was only calculated.

values needed to build the prototype and the measured values of the prototype afterwards. The following Fig. 9 shows the prototype. The switches and the reactive power compensation of the primary site, as printed out in Fig. 4, are placed in the printed circuit board in the top left corner.

With the presented prototype, several measurements are possible. The measurements are divided into two categories and three measured parameters. The measured parameters are the voltage transfer function M_U, presented in Fig. 10, the output power of the system in Fig. 11 and, lastly, the overall efficiency from DC link to DC link with inverter and rectifier, which is printed out in Fig. 12. The two categories stand for measurements of a classical system without any controlling and measurements of the system as it is presented in Fig. 4. The measurement for the classical system is done with a fixed primary side and a fixed secondary side. With these two coils,

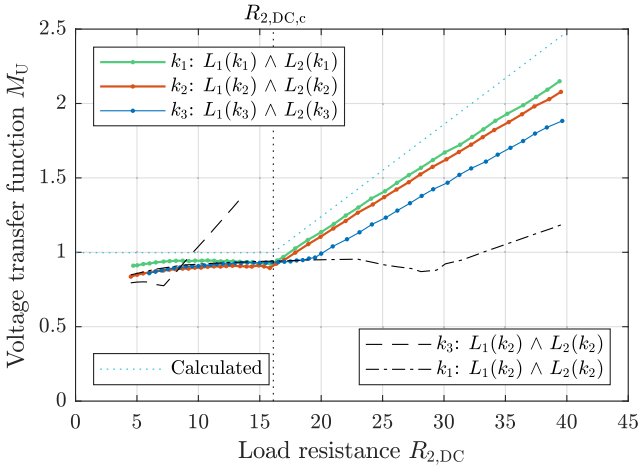

FIGURE 10. Voltage transfer function M_U of the system; measurement for a classical system compared to the system presented in Fig. 4; legend in the northwest refers to the three combinations of L_1 and L_2 optimized for each coupling factor k as presented before; legend in the southeast refers to a classical system with a fixed primary and secondary side coil; vertical dotted line shows the averaged characteristic resistance; dotted line of the legend in the southwest shows the result of the analytical calculation of M_U with (2) and (3) as presented with an A in Fig. 3.

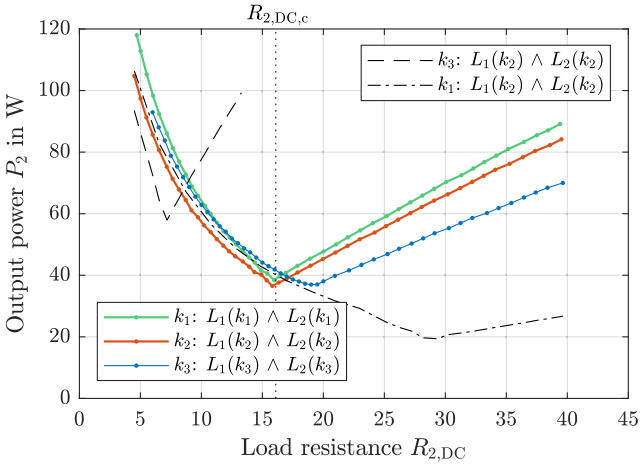

FIGURE 11. Output power of the system with and without controlling as presented in Fig. 4; legend in the southwest refers to the three combinations of L_1 and L_2 optimized for each air gap as presented before; legend in the northeast refers to a classical system with a fixed primary and secondary side coil; vertical dotted line shows the averaged characteristic resistance.

the three operation points as shown in Fig. 3 can be measured. In this specific measurement, the coil pair L_1 and L_2, which is optimized for k_2, is used and the two operating points marked with B in Fig. 3 are measured. Therefore, the secondary side coil is moved to a coupling of k_1 and k_3 instead of coupling k_2 for which it was initially designed.

The measurement of the optimized system should lead to three identical solutions as the theoretical calculation shows. Considering the deviation showed in Table 3, there are some deviations in the measurement as well. Furthermore, the losses in the rectifier and the inverter are not calculated before. Especially the diodes of the inverter lead to a voltage drop, which is quite high in comparison with the used supply

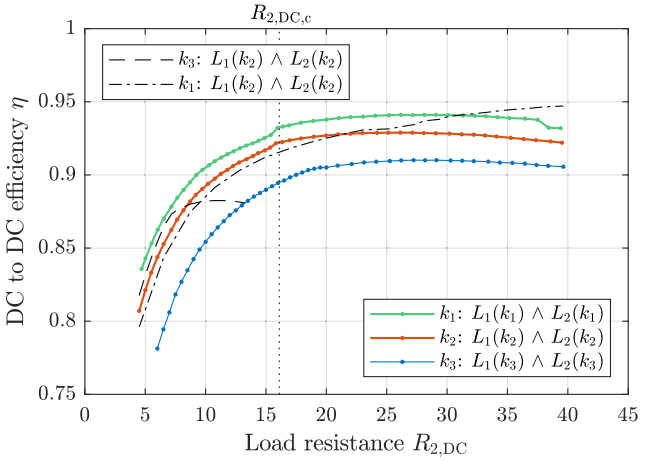

FIGURE 12. Overall efficiency from DC link to DC link of the system; legend in the northwest refers to the three combinations of L_1 and L_2 optimized for each air gap as presented before; legend in the southeast refers to a classical system with a fixed primary side coil; vertical dotted line shows the averaged characteristic resistance.

voltage of only 24 V. Nevertheless, it is visible that the system works well and the difference to a classical system is clearly visible in the measurement. Lastly, the presented efficiency in Fig. 12 shows that the optimized system performs a few percent better than the classical system. The maximum of the efficiency is not exactly at the value of the characteristic resistance as proposed by [21] because losses in inverter and rectifier have an influence which has been neglected in [21].

VI. CONCLUSION

In this paper, a novel method is described to handle different air gaps in contactless energy transfer systems. The measurement shows satisfactory results for a both side serially compensated system as well as for a both side parallel compensated system. In the prototype, no noticeable heating of the used relays was recognized, but the system was not built up with the typical 3.6 kW and more up to now. For a future work the losses in the relay should be taken under examination, since this could cause problems with a high power transfer. The presented system is very economic because it uses only two switches to handle a different coupling factor and, besides, the initial coupling factor measurement, no control system is needed. Due to the tapped primary side coil, the reactive voltage over the single capacitors is much lower as it would be with only one capacitor at the end of the whole coil. Finally, this paper contributes to the general problem of varying coupling factors. Since the standardization is proceeding fast, several new technologies for controlling the systems have a rough ride to be taken into account.

REFERENCES

[1] *Wireless Power Transfer for Light-Duty Plug-In/Electric Vehicles and Alignment Methodology*, Standard J2954, SAE International, 2017. doi: 10.4271/J2954_201711.

[2] *Industry Statement of Charging Interface Initiative e.V. Interoperable Wireless Power Transfer (WPT)*, CharIN-Charging Interface Initiative, Berlin, Germany, 2018.

[3] *Electrically Propelled Road Vehicles—Magnetic Field Wireless Power Transfer—Safety and Interoperability Requirements*, document ISO/PAS 19363:2017, International Organization for Standardization, 2017.
[4] *Electric Vehicle Wireless Power Transfer (WPT) Systems*, Standard IEC 61980-1, International Electrotechnical Commission, Geneva, Switzerland, 2015.
[5] M. Böttigheimer, N. Parspour, and M. Armbruster, "Optimization of the coupling factor curve for lateral offset of a coil pair for contactless inductive charging to generate positioning tolerance," in *Proc. IEEE Int. Conf. Environ. Elect. Eng. IEEE Ind. Commercial Power Syst. Eur. (EEEIC/ICPS Eur.)*, Jun. 2017, pp. 1–8.
[6] C. Joffe, S. Ditze, and A. Rosskopf, "A novel positioning tolerant inductive power transfer system," in *Proc. 3rd Int. Electr. Drives Prod. Conf. (EDPC)*, Oct. 2013, pp. 1–7.
[7] T. Lim and Y. Lee, "Size-adjustable coils for compensation of lateral misalignment in WPT systems," in *Proc. IEEE Wireless Power Transf. Conf. (WPTC)*, Jun. 2018, pp. 1–4.
[8] Y. Li, J. Zhao, Q. Yang, L. Liu, J. Ma, and X. Zhang, "A novel coil with high misalignment tolerance for wireless power transfer," *IEEE Trans. Magn.*, vol. 55, no. 6, Jun. 2019, Art. no. 2800904.
[9] C. Xu, Y. Zhuang, H. Han, C. Song, Y. Huang, and J. Zhou, "Multi-coil high efficiency wireless power transfer system against misalignment," in *Proc. IEEE MTT-S Int. Wireless Symp. (IWS)*, Chengdu, China, May 2018, pp. 1–3.
[10] G. Yang, S. Dong, C. Zhu, R. Lu, G. Wei, and K. Song, "Design of a high lateral misalignment tolerance magnetic coupler for wireless power transfer systems," in *Proc. IEEE PELS Workshop Emerg. Technol., Wireless Power Transf. (WoW)*, May 2017, pp. 34–39.
[11] J. Park, K. Hwang, D. Kim, and S. Ahn, "Lateral misalignment tolerance enhancement by using electromagnet based flux gate in wireless power transfer systems," in *Proc. IEEE Wireless Power Transf. Conf. (WPTC)*, May 2016, pp. 1–4.
[12] T. Diekhans and R. W. D. Doncker, "A dual-side controlled inductive power transfer system optimized for large coupling factor variations and partial load," *IEEE Trans. Power Electron.*, vol. 30, no. 11, pp. 6320–6328, Nov. 2015.
[13] F. P. Wijaya, T. Shimotsu, T. Saito, and K. Kondo, "A simple active power control for a high-power wireless power transmission system considering coil misalignment and its design method," *IEEE Trans. Power Electron.*, vol. 33, no. 11, pp. 9989–10002, Nov. 2018.
[14] S. Sinha, A. Kumar, and K. K. Afridi, "Active variable reactance rectifier—A new approach to compensating for coupling variations in wireless power transfer systems," in *Proc. IEEE 18th Workshop Control Modeling Power Electron. (COMPEL)*, Jul. 2017, pp. 1–8.
[15] H. Widmer, N. Cook, and L. Sieber, "Adaptive wireless energy transfer system," U.S. Patent 2011 285 349, A1, Nov. 24, 2011.
[16] U. Eger, W. Herdeg, and S. Schmitz, "Contactless charging of an electrical energy store of a motor vehicle," U.S. Patent 2014 292 266, A1, Feb. 10, 2014.
[17] D. Maier, J. Heinrich, M. Zimmer, M. Maier, and N. Parspour, "Contribution to the system design of contactless energy transfer systems," in *Proc. IEEE Int. Power Electron. Motion Control Conf. (PEMC)*, Sep. 2016, pp. 1008–1013.
[18] D. Maier, J. Heinrich, M. Zimmer, M. Maier, and N. Parspour, "Contribution to the system design of contactless energy transfer systems," *IEEE Trans. Ind. Appl.*, vol. 55, no. 1, pp. 316–326, Aug. 2018. doi: 10.1109/TIA.2018.2866247.
[19] J. Tritschler, B. Goeldi, S. Reichert, and G. Griepentrog, "Comparison of different control strategies for series-series compensated inductive power transmission systems," in *Proc. 17th Eur. Conf. Power Electron. Appl. (EPE ECCE-Eur.)*, Sep. 2015, pp. 1–8.
[20] K. Aditya and S. S. Williamson, "Comparative study of series-series and series-parallel compensation topologies for electric vehicle charging," in *Proc. IEEE 23rd Int. Symp. Ind. Electron. (ISIE)*, Jun. 2014, pp. 426–430.
[21] M. Zimmer, J. Heinrich, and N. Parspour, "Design of a 3 kW primary power supply unit for inductive charging systems optimized for the compatibility to receiving units with 20 kw rated power," in *Proc. 4th Int. Electr. Drives Prod. Conf. (EDPC)*, 2014, pp. 1–5. [Online]. Available: http://ieeexplore.ieee.org/stamp/stamp.jsp?arnumber=6984415
[22] M. Maier, D. Maier, M. Zimmer, and N. Parspour, "A novel self oscillating power electronics for contactless energy transfer and frequency shift keying modulation," in *Proc. Int. Symp. Power Electron., Elect. Drives, Autom. Motion (SPEEDAM)*, Jun. 2016, pp. 67–72.
[23] D. Zhigang, C. Yuan, and J. A. A. Qahouq, "Reconfigurable magnetic resonance-coupled wireless power transfer system," *IEEE Trans. Power Electron.*, vol. 30, no. 11, pp. 6057–6069, Nov. 2015.
[24] D.-H. Kim, J. Kim, and Y.-J. Park, "Free-positioning wireless power transfer using multiple coupling coils in a transmitter," in *Proc. IEEE-APS Top. Conf. Antennas Propag. Wireless Commun.*, Sep. 2015, pp. 1381–1384.
[25] V. Prasanth, S. Bandyopadhyay, P. Bauer, and J. A. Ferreira, "Analysis and comparison of multi-coil inductive power transfer systems," in *Proc. IEEE Int. Power Electron. Motion Control Conf. (PEMC)*, Sep. 2016, pp. 993–999.
[26] F. Niedermeier, J. Krammer, and B. Schmuelling, "A linear regression based method for estimating magnetic parameters of inductive power transfer systems," in *Proc. IEEE PELS Workshop Emerg. Technol., Wireless Power Transf. (WoW)*, Oct. 2016, pp. 208–213.
[27] L. Liu, Q. Li, L. Liu, and X. Yuan, "Parameter identification of wireless power transfer system using parallel chaos optimization algorithm," in *Proc. Chin. Autom. Congr. (CAC)*, Oct. 2017, pp. 7549–7554.
[28] K. Hata, T. Imura, and Y. Hori, "Simultaneous estimation of primary voltage and mutual inductance based on secondary-side information in wireless power transfer systems," in *Proc. IEEE Wireless Power Transf. Conf. (WPTC)*, May 2016, pp. 1–3.
[29] D. Lin, J. Yin, and S. Y. R. Hui, "Parameter identification of wireless power transfer systems using input voltage and current," in *Proc. IEEE Energy Convers. Congr. Expo. (ECCE)*, Sep. 2014, pp. 832–836.

DAVID MAIER was born in Bühl, Germany, in 1990. He graduated from the Secondary School in Sasbach. He received the bachelor's degree from the Cooperative State University, Stuttgart. He studied Electromobility from the University of Stuttgart, from 2013 to 2015, where he has been with the Institute of Electrical Energy Conversion, since 2016. His research interest includes inductive charging of electric vehicles.

NEJILA PARSPOUR received the master's degree in electrical engineering and the Ph.D. degree *(summa cum laudae)* from Technical University of Berlin, in 1991 and 1995, respectively. She collected five years of industrial experience with Philips and six years of scientific experience with the University of Bremen. She is currently a Professor of electrical energy conversion with the University of Stuttgart and the Head of the Institute of Electrical Energy Conversion. Her research interests and teaching activities include electrical machines and drives with a focus on machine design and contactless energy transfer with a focus on inductive charging systems.